Beyond the CP-curve in Model-based Control of Wind Turbines

Henriksen, Lars Christian; Hansen, Morten Hartvig; Poulsen, Niels Kjølstad

Published in:
Scientific Proceedings of EWEA 2012 - European Wind Energy Conference & Exhibition

Publication date:
2012

Document Version
Publisher's PDF, also known as Version of record

Beyond the CP-curve in Model-based Control of Wind Turbines

L. C. Henriksen
DTU Wind Energy
DK-4000 Roskilde, Denmark
larh@dtu.dk

M. H. Hansen
DTU Wind Energy
DK-4000 Roskilde, Denmark
mhha@dtu.dk

N. K. Poulsen
DTU Informatics
DK-2800 Kgs. Lyngby, Denmark
nkp@imm.dtu.dk

Abstract:

The importance of including dynamic inflow in the model used by the control algorithm is investigated in this contribution. A control setup consisting of a model predictive controller and an extended Kalman filter in conjunction with mechanisms to switch smoothly between partial and full load operation is presented. Results, obtained from high-fidelity simulations, with and without dynamic inflow taken into account by the model-based control setup, show that the inclusion of dynamic inflow is important when operating in conditions close to the rated wind. The presented control setup does not employ collective pitch actuation during partial load operation, for e.g. load mitigation purposes, otherwise dynamic inflow would have been seen to also be of importance for all wind speeds below the rated wind speed.

Keywords: dynamic inflow, model-based control, model-based state estimation.

1 Introduction

Dynamic inflow describes the lag with which the wake induced by a wind turbine settles to a new equilibrium when operating conditions of the wind turbine are changed, e.g. a sudden change in pitch angle. Dynamic inflow has long been recognized as a significant phenomenon which should be taken into account when modelling wind turbines in e.g. aero-servo-elastic codes [1–3]. The importance of dynamic inflow is not new knowledge for the wind energy community in general as the cited works are dated to the late 1980s and early 1990s. It has already been established that taking the dynamic inflow into account when designing a controller leads to reduced loads [4] and classic proportional-integral controllers have been tuned to achieve certain closed-loop properties by taking the dynamic inflow into account [5]. But for model-based control and state estimation methods applied to wind turbines the quasi-static power and thrust coefficients, usually denoted C_P and C_T, are most often used [6–10].

Model-based control and state estimation require a simple aerodynamic model which is usually based on blade element momentum theory (BEM). In reality temporal dynamics on several time scales occur, giving rise to dynamic inflow on the slow end of the time scale and dynamic stall on the fast end of the time scale. In this work a simple dynamic inflow model inspired by the model proposed by Øye [1] and also described in Hansen [11] and Snel and Schepers [3] has led to the development of an even simpler dynamic inflow model suited for model-based control and state estimation purposes.

A model-based control setup has been developed, which is able to handle both partial and full load operation. The state space model used by the control setup can include either a quasi-static or a dynamic inflow aerodynamic model. The performance of the model-based control setup based on each of the aerodynamic models is tested in the aero-servo elastic code HAWC2 [12, 13] and is compared to a benchmark proportional-integral controller.

The paper is structured in the following order: The control design model, including the simplified dynamic wake model, is presented in Section 2. A brief introduction to the implemented controller can be found in Section 3. Finally, results are presented and discussed in Section 4 and conclusions are drawn in Section 5.

2 Model for controller design

In this section the model used by the extended Kalman filter and the model predictive controller is presented. The submodels constituting the full control design model are explained in Sections 2.1 to 2.4. The combination of the submodels into a full model and the linearization of the nonlinear model is explained in 2.5. In 2.6 the presented control design model is compared to results obtained from HAWC2 [13]. The presented model allows for individual and cyclic pitch control, although only collective pitch control has been investigated in this work. The Coleman transformation [14–16] also known as the multi-blade transformation is applied on the control design model. The reader is requested to consult e.g. [17] for detailed description of the implementation details

regarding the multi-blade transformation applied on the control design model and the control and state estimation algorithm.

2.1 Structural model

The structural model used by the control algorithm is based on Lagrangian mechanics. Tilt of the shaft and coning of the blades is omitted in this simplified control design model and all the axes along the blade span, e.g. center of gravity, are assumed to coincide with the blade pitching axis. Also, the influence of gravity has been omitted.

Blade structural degrees-of-freedom have not been included in the model, future work could investigate the potential benefits of including blade flexibility, but blade root bending moments sensors such as strain gauges are used as sensors.

The Cartesian coordinate system used in this model is similar to HAWC2 with the z-axis is positive in downwards direction and y-axis is positive in wind direction. The bottom of the wind turbine tower is defined as

$$\boldsymbol{r_0} = \begin{bmatrix} r_0^x \\ r_0^y \\ r_0^z \end{bmatrix} = \begin{bmatrix} 0 \\ 0 \\ 0 \end{bmatrix} \tag{1}$$

and is the base in local Cartesian coordinate system describing the position of the structural components of the wind turbine. The nacelle center $\boldsymbol{r_n}$

$$\boldsymbol{r_n} = \boldsymbol{r_0} + \begin{bmatrix} 0 \\ \psi_{fa} \\ -H_t \end{bmatrix} \tag{2}$$

where H_t is height of tower and ψ_{fa} is the fore-aft degree-of-freedom of the tower. The position at radius r of blade k is given as

$$\boldsymbol{r_{b},i}(r) = \boldsymbol{r_n} + \begin{bmatrix} 0 \\ -L_s \\ 0 \end{bmatrix} + \begin{bmatrix} \cos\phi_i & 0 & \sin\phi_i \\ 0 & 1 & 0 \\ -\sin\phi_i & 0 & \cos\phi_i \end{bmatrix} \begin{bmatrix} \cos\theta_{e,i}(r) & -\sin\theta_{e,i}(r) & 0 \\ \sin\theta_{e,i}(r) & \cos\theta_{e,i}(r) & 0 \\ 0 & 0 & 1 \end{bmatrix} \begin{bmatrix} 0 \\ 0 \\ r \end{bmatrix} \tag{3}$$

where L_s is the length of the drive-shaft. The effective pitch angle of blade i is the sum of the controlled pitch angle and the twist

$$\theta_{e,i}(r) = \theta_i + \theta_b(r) \tag{4}$$

The azimuth angle of the rotor is defined as the azimuth angle of blade 1

$$\phi_r = \phi_g + \phi_\Delta \tag{5}$$

where ϕ_g is generator-side low speed shaft rotational degree-of-freedom and ϕ_Δ is the torsional degree-of-freedom of the low speed shaft. The temporal derivatives are defined $\dot{\phi}_r \equiv \Omega_r$, $\dot{\phi}_g \equiv \Omega_g$.The azimuth angle of blade i is given as

$$\phi_i = \phi_r + \tfrac{2\pi}{3}(1-k) \tag{6}$$

The Lagrangian is defined as

$$\mathcal{L} = \mathcal{T} - \mathcal{V} \tag{7}$$

The following notation is introduced to ease notation

$$\|\boldsymbol{q}\|_{\mathbf{Q}}^2 = \boldsymbol{q}^T\mathbf{Q}\boldsymbol{q}$$

and is used in Sections 2 and 3. The total kinetic energy of the wind turbine is

$$\mathcal{T} = \tfrac{1}{2}\|\dot{\boldsymbol{r}}_{\boldsymbol{n}}\|_{M_t}^2 + \tfrac{1}{2}\|\Omega_g\|_{I_g}^2 + \tfrac{1}{2}\|\Omega_r\|_{I_h}^2 + \sum_{k=1}^{n_b}\tfrac{1}{2}\int_0^R \|\dot{\boldsymbol{r}}_{\boldsymbol{b},i}(r)\|_{m_b(r)}^2 dr \tag{8}$$

where M_t is the equivalent tower top mass, I_g and I_h are inertial mass of generator and rotor hub, respectively. And $m_b(r)$ is the radially distributed blade mass. The total potential energy of the wind turbine is

$$\mathcal{V} = \tfrac{1}{2}\|\psi_{fa}\|_{K_t}^2 + \tfrac{1}{2}\|\phi_\Delta\|_{K_s}^2 \tag{9}$$

where K_t and K_s are tower and drive shaft stiffness, respectively. Spring stiffnesses etc. have been been calculated [18] from distributed data given in [19]. The structural model contains n_q degrees-of-freedom

$$\boldsymbol{q} = [\phi_g \ \phi_\Delta \ \psi_{fa}]^T \tag{10}$$

The equations of motion also known as the Lagrange equations are

$$\frac{d}{dt}\left(\frac{\partial \mathcal{L}}{\partial \dot{q}_j}\right) - \frac{\partial \mathcal{L}}{\partial q_j} + \frac{\partial \mathcal{D}}{\partial \dot{q}_j} = Q_j, \quad j = 1, \ldots, n_q \tag{11}$$

where the dissipative energy function is $\mathcal{D} = \frac{1}{2}\dot{\boldsymbol{q}}^T\mathbf{D}\dot{\boldsymbol{q}}$. The generalized non-conservative forces acting on the wind turbine are the individual radially distributed blade forces $\boldsymbol{F}_{\boldsymbol{b},i}(r)$ and the generator torque Q_g

$$Q_j = \sum_{k=1}^{n_b}\int_0^R \frac{\partial \boldsymbol{r}_{\boldsymbol{b},i}(r)}{\partial q_j}\cdot \boldsymbol{F}_{\boldsymbol{b},i}(r)dr + \frac{\partial \phi_g}{\partial q_j}Q_g \tag{12}$$

where the individual blade forces are projected from the local blade coordinate system to the global coordinate system as a function of the individual blade azimuth angle ϕ_i

$$\boldsymbol{F}_{\boldsymbol{b},i}(r) = \begin{bmatrix} \cos\phi_i & 0 \\ 0 & 1 \\ -\sin\phi_i & 0 \end{bmatrix} \begin{bmatrix} F_{t,i}(r) \\ F_{n,i}(r) \end{bmatrix} \tag{13}$$

The calculations of the local blade forces is given by (26), which is based blade element momentum theory and is elaborated in Section 2.3.1.

The individual blade sensors denoted blade edge (be) and blade flap (bf) are calculated by

$$Q^{SG}_{bf,i} = \int_0^R \varphi_{bf}(r) F_{bf,i}(r)\, dr \tag{14a}$$

$$Q^{SG}_{be,i} = \int_0^R \varphi_{be}(r) F_{be,i}(r)\, dr \tag{14b}$$

where $\varphi_{bf}(r)$ and $\varphi_{be}(r)$ are shape functions calculated using beam theory [18] and where the point forces projected onto the blade plane are given by (27).

2.2 Wind turbulence model

The wind field in the control design model is assumed to be given by linear horizontal and vertical shears added to the rotor-wide mean wind speed. The radially dependent wind speed of blade i is given by

$$V_i(r) = v_i \frac{r}{R} + V_0 \tag{15}$$

where V_0 is the rotor-wide mean wind speed and v_i is difference between the free wind speed at the tip of blade i and V_0. Under deterministic conditions and simplified conditions where the linear shear assumption is valid, the time-varying wind speeds affecting the individual blades can be transformed to time-constant values in the fixed-frame coordinate system

$$\boldsymbol{V^f} = \mathbf{M}(\phi_r)\boldsymbol{V} \tag{16}$$

where $\boldsymbol{V^f} = [V_0\ V_c^f V_s^f]$, is the fixed-frame wind speed vector representing mean wind speed, vertical shear and horizontal shear, respectively. $\boldsymbol{V} = [V_1(R)\ V_2(R)\ V_3(R)]^T$ is the rotating frame wind speed vector and $\mathbf{M}(\phi_r)$ is the multi-blade transformation matrix [17]. For a more realistic wind field with e.g. a power law wind shear, tower shadow and turbulence the model fixed-frame wind speeds $\boldsymbol{V^f}$ are also time-varying. In [20] it can be seen that the wind speeds in the fixed-frame have significant content around the 3P, 6P etc. frequencies. The harmonic content can be included in the control design model giving

$$\boldsymbol{V}^f = \boldsymbol{v}^f + \bar{\boldsymbol{V}}^f \tag{17}$$

where $\bar{\boldsymbol{V}}^f$ are slowly updated model parameters around which the dynamic output

$$\boldsymbol{v}^f = \boldsymbol{v}^f_{3P} + \boldsymbol{v}^f_{6P} + \dots \tag{18}$$

perturbs. In this work only the 3P content has been included in the control design model, so $\boldsymbol{v}^f = \boldsymbol{v}^f_{3P}$, giving

$$\ddot{v}^f_i + 2\zeta_v\omega_v\dot{v}^f_i + \omega_v^2 v^f_i = \omega_v^2 e_i, \quad e_i \in N(0,\sigma_i^2) \tag{19}$$

where $i = 0, c, s$. The damping ratio ζ_v has been chosen to be 0.01. The natural frequency of the 3P wind turbulence model is given by $\omega_v = 3\Omega/\sqrt{1-\zeta_v^2}$.

2.3 Aerodynamic model

In this section, the aerodynamic model included in the control design model is presented. Blade element momentum theory is revisited in 2.3.1 and the quasi-steady control design model is documented in 2.3.2. The newly developed simplified dynamic inflow model suitable for model-based control and state estimation algorithms is briefly explained in 2.3.3.

2.3.1 Blade element momentum theory

Blade element momentum (BEM) theory describes the aerodynamic forces at a finite number of blade elements along the blade span. The aerodynamic forces induce an air flow in the opposite direction and tangential to the free wind speed to fulfill the equilibrial condition. Fig. 1 gives an overview of the velocity triangle in a single blade element.

The relative wind speeds for an element on blade i at radial distance r, normal and tangential to the rotor plane, respectively, are given by

$$V_{n,rel,i}(r) = V_i(r) - \dot{r}^y_{b,i}(r) \tag{20a}$$

$$V_{t,rel,i}(r) = \sqrt{\left(\dot{r}^z_{b,i}(r)\right)^2 + \left(\dot{r}^x_{b,i}(r)\right)^2} \tag{20b}$$

To simplify notation, structural degrees-of-freedom and wind shear are subsequently omitted, yielding $V_{n,rel,i}(r) = V$ and $V_{t,rel,i}(r) = \Omega r$.

The induced velocities tangential v_t and normal v_n to the rotor plane are described by the induction factors a_t and a_n, the resulting inflow velocity in the nor-

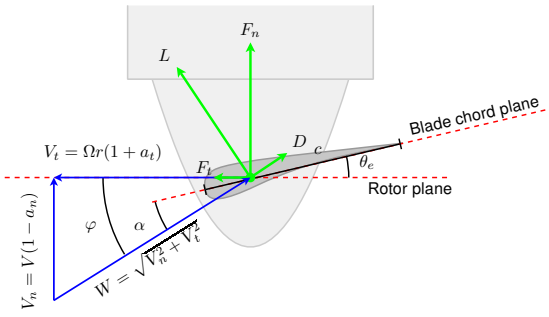

Figure 1: Cross section of blade in the span wise direction along the blade.

mal and tangential directions is

$$V_n = V - v_n = V(1 - a_n),\ v_n = Va_n \tag{21}$$
$$V_t = \Omega r + v_t = \Omega r(1 + a_t),\ v_t = \Omega r a_t \tag{22}$$

The absolute value of the inflow velocity seen by the blade and the inflow angle are

$$W = \sqrt{V_n^2 + V_t^2} \tag{23a}$$
$$\varphi = \arctan \frac{V_n}{V_t} \tag{23b}$$

The angle of attack is the difference between the inflow angle and the effective pitch of the blade element

$$\alpha = \varphi - \theta_e \tag{24}$$

The velocity triangle displayed in Fig. 1 gives the aerodynamic forces where drag D is parallel to the inflow velocity and lift L is normal to the inflow velocity. Lift and drag, when neglecting unsteady local effects from shed vorticity, added mass and dynamic stall, is given by

$$L = \frac{1}{2}\rho W^2 C_L(\alpha)c \tag{25a}$$
$$D = \frac{1}{2}\rho W^2 C_D(\alpha)c \tag{25b}$$

Lift and drag can be projected into forces tangential F_t and normal F_n to the rotor plane

$$F_n = L\cos\varphi + D\sin\varphi \tag{26a}$$
$$F_t = L\sin\varphi - D\cos\varphi \tag{26b}$$

and to the local blade plane

$$F_{bf} = L\cos\alpha + D\sin\alpha \tag{27a}$$
$$F_{be} = L\sin\alpha - D\cos\alpha \tag{27b}$$

2.3.2 Quasi-steady aerodynamic model

The blade forces (26) and (27), where structural degrees-of-freedom and wind shear is included, can be written in a general form as

$$F_x(V_{n,rel,i}(r), V_{t,rel,i}(r), \theta_i, v_{n,i}(r), v_{t,i}(r), r) \tag{28}$$

where the induced wind speeds $v_{n,i}(r)$ and $v_{t,i}(r)$ are found in steady state by calculating the radially distributed quasi-steady induction factors, $a_{n,i}^{qs}(r)$ and $a_{t,i}^{qs}(r)$, computed with the BEM algorithm [11], where Prandtl's tip-loss correction and Glauert's axial induction correction are taken into account. There are several versions of Glauert's axial induction correction for high induction factors and slightly different quasi-steady axial induction factors are found depending on which model is used. The axial induction factor correction for high axial induction factors used in this work is the same as the one used in HAWC2 [21].

In this work, the quasi-steady axial induction factors have been calculated off-line assuming no wind shear and a rigid structure. The tip-speed-ratio $\lambda_i = V_{t,rel,i}(R)/V_{n,rel,i}(R)$ enables a two-dimensional (λ_i, θ_i) description of the steady state aerodynamic forces rather than a three-dimensional $(V_{n,rel,i}(R), V_{t,rel,i}(R), \theta_i)$. The induced wind speeds used by (28) for the quasi-steady aerodynamic model are

$$v_{n,i}(r) = V_{n,rel,i}(r)a_{n,i}^{qs}(\lambda_i, \theta_i, r) \tag{29a}$$
$$v_{t,i}(r) = V_{t,rel,i}(r)a_{t,i}^{qs}(\lambda_i, \theta_i, r) \tag{29b}$$

2.3.3 Simplified dynamic inflow aerodynamic model

The dynamic inflow model used in this work is based on the single-state dynamic inflow model proposed in [22]. The local tangential induced velocities are assumed quasi-steady and obtained from (29b). The local axial induced velocities $v_{n,i}(r)$ are given by the averaged induced axial velocity $\bar{v}_{n,i}$ and the quasi-steady distribution of the axial induction factor

$$v_{n,i}(r) = \frac{a_n^{qs}(\lambda_i, \theta_i, r)}{\bar{a}_n^{qs}(\lambda_i, \theta_i)}\bar{v}_{n,i} \tag{30}$$

where

$$\bar{a}_n^{qs}(\lambda_i, \theta_i) = \frac{1}{R}\int_0^R a_n^{qs}(\lambda_i, \theta_i, r)dr \tag{31}$$

The temporal dynamics of the averaged axial induced velocity is governed by a first order ordinary differential equation

$$\tau_i\dot{\bar{v}}_{n,i} + \bar{v}_{n,i} = V_{n,rel,i}(R)\bar{a}_n^{qs}(\lambda_i, \theta_i) \tag{32}$$

inspired by [1] the time constant is given as

$$\tau_i = \frac{1}{2}\frac{1.1R}{V_{n,rel,i}(R) - 1.3\bar{v}_{n,i}} \tag{33}$$

based on the same assumption as in [22].

2.4 Actuators

The actuators are assumed linear under the assumption that a low level controller, e.g. PID or some type of nonlinear controller, is operating in closed loop with the actuator mechanics. The closed loop actuator is described with second order dynamics

$$\ddot{\theta}_i + 2\zeta_\theta\omega_\theta\dot{\theta}_i + \omega_\theta^2\theta_i = \omega_\theta^2\theta_{i,ref} \tag{34a}$$

subject to

$$\begin{bmatrix}\theta_{min}\\ \dot{\theta}_{min}\end{bmatrix} \le \begin{bmatrix}\theta_i\\ \dot{\theta}_i\end{bmatrix} \le \begin{bmatrix}\theta_{max}\\ \dot{\theta}_{max}\end{bmatrix} \tag{34b}$$

where ω_θ and ζ_θ are the natural frequency and damping ratio of the actuator and θ_{ref} is the reference signal from the controller. The generator torque actuator is assumed to be described with first order dynamics

$$\tau_g \dot{Q}_g + Q_g = Q_{g_{ref}} \tag{35a}$$

subject to

$$\begin{bmatrix} Q_{g,min} \\ \dot{Q}_{g,min} \end{bmatrix} \leq \begin{bmatrix} Q_g \\ \dot{Q}_g \end{bmatrix} \leq \begin{bmatrix} Q_{g,max} \\ \dot{Q}_{g,max} \end{bmatrix} \tag{35b}$$

where τ_g is the time constant of the generator torque actuator and $Q_{g_{ref}}$ is the reference signal from the controller.

2.5 Combined model and linearization

The ordinary differential equations of the submodels, excluding the wind turbulence model, are gathered in a state space ordinary differential equation function and transformed to the multi-blade coordinate system. The wind turbine model is then augmented with the wind turbulence model, which is already in the multi-blade coordinate system. The full model is time-discretized to obtain the state progress equation

$$\boldsymbol{x}_{k+1} = \underline{\boldsymbol{f}}(\boldsymbol{x}_k, \boldsymbol{u}_k) \tag{36a}$$

and the ouputs are gathered in an output state space function

$$\boldsymbol{y}_k = \boldsymbol{g}_{\boldsymbol{y}}(\boldsymbol{x}_k, \boldsymbol{u}_k) \tag{36b}$$

where $\boldsymbol{x}$ is the state vector, $\boldsymbol{u}$ is the input vector and $\boldsymbol{y}$ is the measurement vector. The vectors are comprised by the following variables

$$\boldsymbol{x} = [\Omega_r \; \Omega_g \; \phi_\Delta \; \psi_{fa} \; \dot{\psi}_{fa} \; \bar{v}_{n,i} \; \theta_i \; \dot{\theta}_i \; Q_g \; v_i^f \; \dot{v}_i^f]^T$$
$$\boldsymbol{u} = [\theta_{ref,i} \; Q_{g,ref}]^T$$
$$\boldsymbol{y} = [\Omega_r \; \Omega_g \; \phi_\Delta \; \ddot{\psi}_{fa} \; Q_{bf,i}^{SG} \; Q_{be,i}^{SG} \; \theta_i \; \dot{\theta}_i \; \ddot{\theta}_i \; Q_g \; \dot{Q}_g \; P_e]^T$$

In section 3 additional output vectors such as soft and hard constraints are also used, these vector output functions are constructed in manner similar to (36b). The algorithms presented in section 3 are based on linear assumptions, the Jacobians of (36) with regards to $\boldsymbol{x}$ and $\boldsymbol{u}$ are computed through numerical differentiation.

2.6 Comparison of control design model and HAWC2

Figures 2 and 3 show the Bode plots of the transfer functions from collective pitch and generator torque to generator speed, rotor speed and tower top fore-aft displacement at mean wind speeds of 8 m/s and 16 m/s, respectively. During partial load operation (c.f. Figure 2), the importance of dynamic inflow is seen in the Bode plot depicting the transfer function from collective pitch angle to rotor and generator speed. During full load operation (c.f. Figure 3), dynamic inflow is seen not to have any significant influence.

It can furthermore be seen, both in Figure 2 and 3, that at higher frequencies the control design model does not fit with the more complex HAWC2 model. This is mainly caused by the omission of blade edge degree-of-freedom in the control design model as the blade edge couples with the drive-shaft degree-of-freedom and gives a more complex behavior. In recognition of this poor fit for high frequencies the control design model used by the controller in Section 3.2 has been augmented with frequency dependent weights on the control signals, thus avoiding high frequency actuation which could lead to excitation of poorly modeled modes.

3 Controller

In this section the implemented controller is briefly presented. The overall setup of the control, state estimation and switching blocks is depicted in Figure 4. The control and state estimation algorithms are presented in subsections 3.2 and 3.1, respectively. It can briefly be mentioned that during partial load operation the controller seeks to track the optimal tip-speed ratio by tracking the generator speed as a function of the estimated wind speed. The collective pitch angle is kept constant at its optimal value during partial load operation. During full load operation the controller seeks to keep the generator speed and power at their nominal values. For details regarding the switching mechanism and further details regarding the control and state estimation algorithms [22] can be consulted.

The control and estimation blocks are based on a nonlinear state space model of the wind turbine as described in Section 2. The model can either assume quasi-steady or dynamic inflow aerodynamics as described in Sections 2.3.2 and 2.3.3, respectively. Furthermore, the control design model has been augmented with high-pass filters of the control input rates $\dot{\boldsymbol{u}}$, such that a frequency dependent weight can be put on the control actuation. In each sample the nonlinear model is linearized according to the current operating point and the linearized model is used by the control and estimation algorithms.

3.1 Extended Kalman filter and disturbance model

To ensure off-set free performance, the control design model (36) can be augmented with a distur-

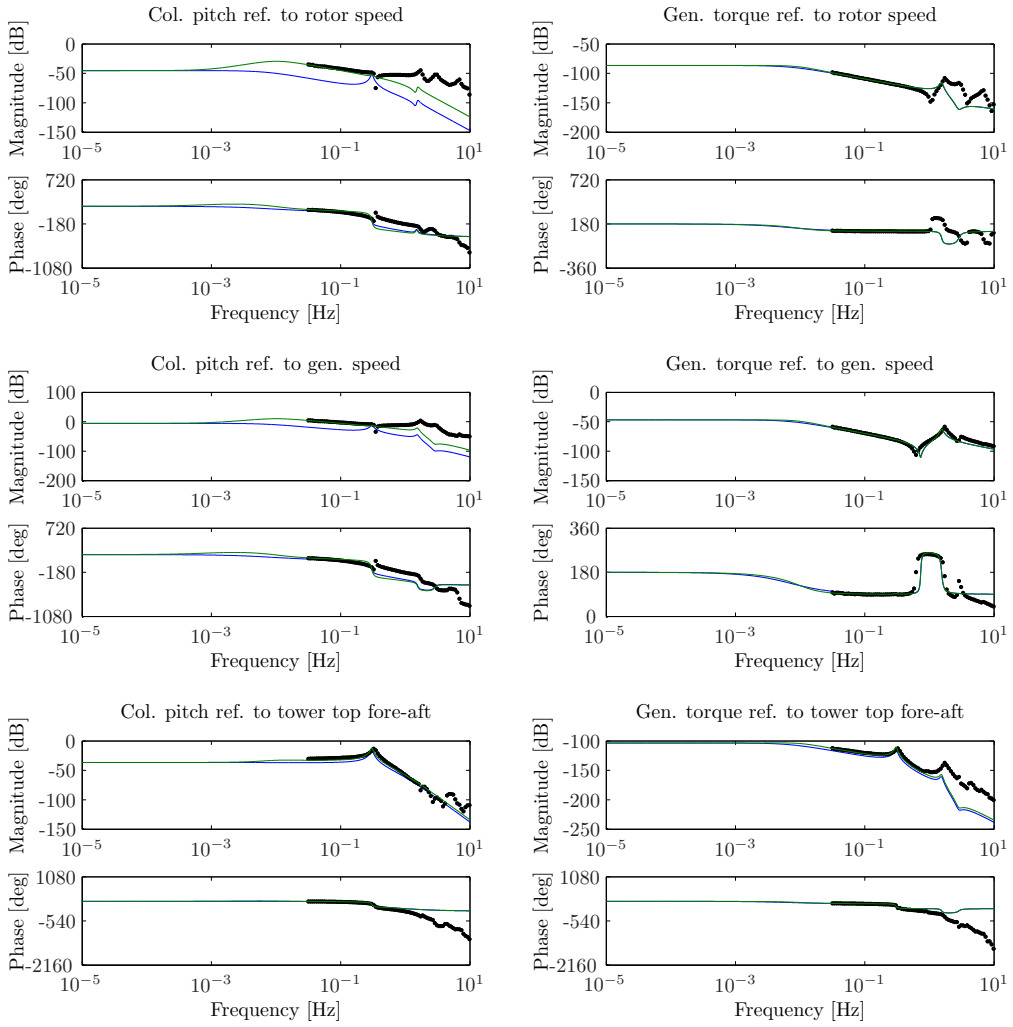

Figure 2: Transfer functions at a mean wind speed of 8 m/s. Black dots are obtained from HAWC2. Blue line is obtained from control design model with a quasi-steady aerodynamic model. Green line is obtained from control design model with a simplified dynamic inflow aerodynamic model.

bance model, which is used to compensate for actual disturbances and for any plant/model mismatch

$$\begin{bmatrix} \boldsymbol{x} \\ \boldsymbol{d} \\ \boldsymbol{p} \end{bmatrix}_{k+1} = \begin{bmatrix} \underline{\boldsymbol{f}}(\boldsymbol{x}_k, \boldsymbol{u}_k) + \mathbf{E}\boldsymbol{d}_k \\ \boldsymbol{d}_k \\ \boldsymbol{p}_k \end{bmatrix} + \begin{bmatrix} \boldsymbol{w}_{\boldsymbol{x}} \\ \boldsymbol{w}_{\boldsymbol{d}} \\ \boldsymbol{w}_{\boldsymbol{p}} \end{bmatrix}_k \tag{37a}$$

$$\boldsymbol{y}_k = \boldsymbol{g}_{\boldsymbol{y}}(\boldsymbol{x}_k, \boldsymbol{u}_k) + \mathbf{F}_{\mathbf{y}}\boldsymbol{p}_k + \boldsymbol{v}_k \tag{37b}$$

where $\boldsymbol{w}_{\boldsymbol{x}}$ $\boldsymbol{w}_{\boldsymbol{d}}$ $\boldsymbol{w}_{\boldsymbol{p}}$ and $\boldsymbol{v}$ is assumed to be zero-mean Gaussian distributed white noise and $\boldsymbol{d}$ are state disturbances and $\boldsymbol{p}$ are output disturbances interconnected with (36) through the disturbance model $(\mathbf{E}, \mathbf{F}_{\mathbf{y}})$. Further details regarding the extended Kalman filter (EKF) and the disturbance model can be found in [22].

3.2 Relinearized Model Predictive Control

In this section, the estimated state vector provided by the extended Kalman filter is denoted $\hat{\boldsymbol{x}}$. The estimated disturbances $\hat{\boldsymbol{d}}$ and $\hat{\boldsymbol{p}}$ are assumed to be constant contributions and are used as parameters rather than dynamic states.

The outputs used in this section $\boldsymbol{g}_{\boldsymbol{r}}(\cdot)$, $\boldsymbol{g}_{\boldsymbol{z}}(\cdot)$, $\boldsymbol{g}_{\boldsymbol{s}}(\cdot)$ and $\boldsymbol{g}_{\boldsymbol{h}}(\cdot)$, coinciding with the measured outputs $\boldsymbol{g}_{\boldsymbol{y}}(\cdot)$, are corrected by the estimated outputs disturbances $\hat{\boldsymbol{p}}$. This is done by inserting coinciding rows of the output disturbance matrix $\mathbf{F}_{\mathbf{y}}$ in the matrices $\mathbf{F}_{\mathbf{r}}$, $\mathbf{F}_{\mathbf{z}}$, $\mathbf{F}_{\mathbf{s}}$ and $\mathbf{F}_{\mathbf{h}}$, which are otherwise padded with zeros.

The relinearized model predictive controller (RLMPC) entails the computation of the control signal within a prediction horizon in the range $\mathbb{K} = (0, \ldots, \infty)$. The RLMPC is formulated as a dual mode horizon where the first part, i.e $\mathbb{K}^{N-1} = (0, \ldots, N-1)$, is considered constrained. In the second horizon, i.e. $\mathbb{K}^{\infty} = (N, \ldots, \infty)$, it is assumed that the plant has reached a state where the unconstrained solution is feasible.

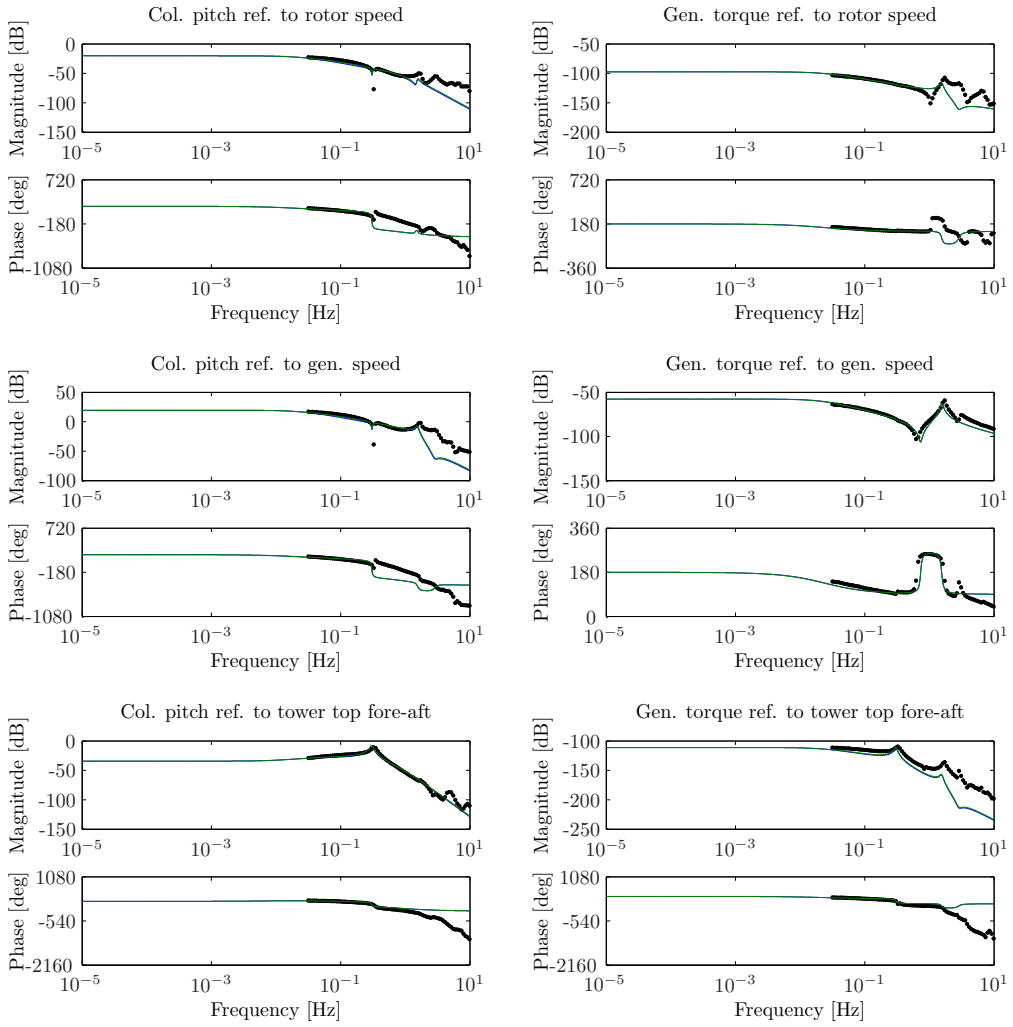

Figure 3: Transfer functions at a mean wind speed of 16 m/s. Black dots are obtained from HAWC2. Blue line is obtained from control design model with a quasi-steady aerodynamic model. Green line is obtained from control design model with a simplified dynamic inflow aerodynamic model.

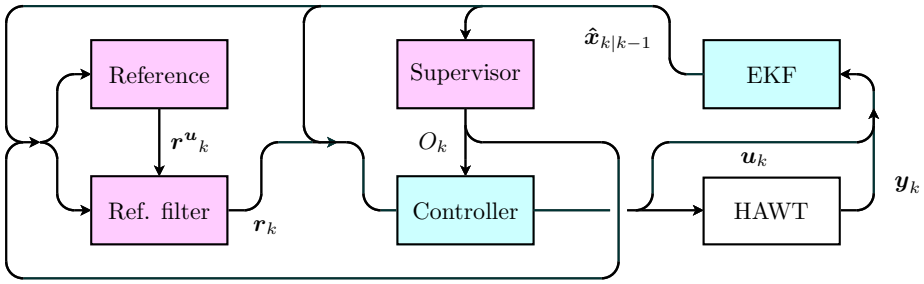

Figure 4: Setup of the hybrid controller. An extended Kalman filter (EKF) provides estimates of states used by other blocks in the diagram. Supervisor block provides partial or full load control objectives to controller depending on switching conditions. Reference and reference filter blocks provide references for the controller to track depending on whether partial or full load operation is active.

The dual mode optimization problem is

$$\min \sum_{k\in\mathbb{K}^{\infty}} \phi_k(\boldsymbol{x}_k,\boldsymbol{u}_k,\hat{\boldsymbol{p}}) + \sum_{k\in\mathbb{K}^{N-1}} \phi_k(\boldsymbol{x}_k,\boldsymbol{u}_k,\hat{\boldsymbol{p}}) + \sum_{k\in\mathbb{K}^{N-1}} \frac{1}{2}\|\boldsymbol{\sigma}_k\|^2_{\mathbf{W}_\sigma} \tag{38a}$$

subject to the state progress equality constraint

$$\boldsymbol{x}_k = \hat{\boldsymbol{x}}, \qquad k = 0 \tag{38b}$$

$$\boldsymbol{x}_{k+1} - \underline{\boldsymbol{f}}(\boldsymbol{x}_k,\boldsymbol{u}_k) = \mathbf{E}\hat{\boldsymbol{d}}, \qquad k \in \mathbb{K} \tag{38c}$$

and the soft and hard inequality constraints

$$\boldsymbol{g_s}(\boldsymbol{x}_k) - \boldsymbol{\sigma}_k \leq \boldsymbol{s} - \mathbf{F_s}\hat{\boldsymbol{p}}, \qquad k \in \mathbb{K}^{N-1} \tag{38d}$$

$$\boldsymbol{g_h}(\boldsymbol{x}_k, \boldsymbol{u}_k) \leq \boldsymbol{h} - \mathbf{F_h}\hat{\boldsymbol{p}}, \qquad k \in \mathbb{K}^{N-1} \tag{38e}$$

where the stagewise cost function

$$\begin{aligned}\phi_k(\boldsymbol{x}_k, \boldsymbol{u}_k, \hat{\boldsymbol{p}}) = \frac{1}{2}\|\boldsymbol{g_z}(\boldsymbol{x}_k, \boldsymbol{u}_k) + \mathbf{F_z}\hat{\boldsymbol{p}}\|^2_{\mathbf{W_z}} \\ + \frac{1}{2}\|(\boldsymbol{r} - \boldsymbol{g_r}(\boldsymbol{x}_k, \boldsymbol{u}_k)) + \mathbf{F_r}\hat{\boldsymbol{p}}\|^2_{\mathbf{W_r}}\end{aligned}$$

consist of two terms: The first term seeks to minimize dynamic variations given by $\boldsymbol{g_z}(\cdot)$ such as e.g. velocities, accelerations. The second term seeks to drive the plant reference outputs $\boldsymbol{g_r}(\cdot)$ towards the desired reference $\boldsymbol{r}$, e.g. generator power and generator speed. An additional cost term, only included in the first part of the prediction horizon, seeks to minimize the violation of the soft constraints $\boldsymbol{\sigma}$. The weight matrices $\mathbf{W_r}$, $\mathbf{W_z}$ and $\mathbf{W}_\sigma$ are diagonal matrices whose elements are dependent on whether partial or full load operation is active.

4 Results

The proposed controller design is tested on the NREL 5MW reference wind turbine [19] in the aero-servo-elastic code HAWC2 [13] and compared to a benchmark PI-based controller proposed by Jonkman et al. [19]. Two different control configurations are compared MPC1 and MPC2, respectively. MPC1 has weights in the cost function on generator power and generator speed as well as weights on the control rate signals. MPC2 is similar to MPC1 but has a reduced weight on generator speed tracking. Both configurations are tested both with a quasi-static and a dynamic inflow model included in the model used by the controller, giving a total of four different control setups.

Simulations for different mean speeds, covering the full range of operation for the wind turbine, have been performed. For each mean wind speed four turbulence seeds have been used. The turbulent wind field used in the simulations is presented in Mann [23] with class A turbulence intensity as defined in [24], and a wind shear with a power coefficient of 0.2 is used together with a potential flow tower shadow model.

Two different sensors are used for comparison of fatigue loads: Tower base fore-aft and torsion of the low speed drive train shaft. The fatigue load calculations are based on the standard defined in [25]. For both sensors a material number of 3, equivalent to steel, is used.

Another measure of control performance is to compare the root-mean-square (RMS) of selected signals. The RMS error of generator speed and power relative to their nominal values have also been calculated. The standard deviation (Std.) of the generator torque rate and pitch travel give some insight into how active the different control configurations are.

Fig. 5 shows the results for the different controllers. Each point on the plots is the mean value obtained from the 4 different turbulence seeds.

MPC1, which is tuned aggressively, is sensitive to the modelling error caused by quasi-static aerodynamics which is clearly seen in Fig. 5. In an attempt to regulate the generator speed as prescribed by the weight in the cost function the pitch travel around rated wind speed is significantly increased, for the controller assuming quasi-steady aerodynamics, leading to significantly increased tower loads.

It can also be observed that the standard deviation of generator torque rate for MPC1 and MPC2 cross each around rated wind speed. This is because MPC1 has a high weight on generator speed tracking and since pitch is not used during partial load the generator torque has to be more active at partial load. For full load the pitch comes into effect and alleviates the generator torque actuator.

MPC2, which is tuned less aggressive, is not as sensitive to the modelling error and the inclusion of dynamic inflow is not as important as for the aggressively tuned MPC1.

The axial induction is at its highest during partial load where the effect of dynamic inflow is most noticeable when pitching the blades. As neither the MPC1 nor the MPC2 have any pitch actuation at partial load operation the effect of dynamic inflow is most significant just above rated wind speed where the axial induction is still quite high and the pitching of blades is active.

5 Conclusion

In the presented work a wind turbine has been controlled with collective blade pitch and generator torque by a model-based control setup. The importance of including dynamic inflow in the control design model used by the state estimator and control algorithm has been investigated by comparing two sets of controllers. The first set has been tuned to track generator speed aggressively leading to increased blade pitch actuation, compared to the second set, which has been tuned less aggressively. Results show that dynamic inflow is an important model component for controllers, in particular around rated wind speed, for controllers which have been tuned to have a high bandwidth.

For advanced model-based control setups where pitch actuation is active during partial load operation dynamic inflow should be included in the control design model. This could especially be relevant for preview-based (e.g. Lidars) control strategies at-

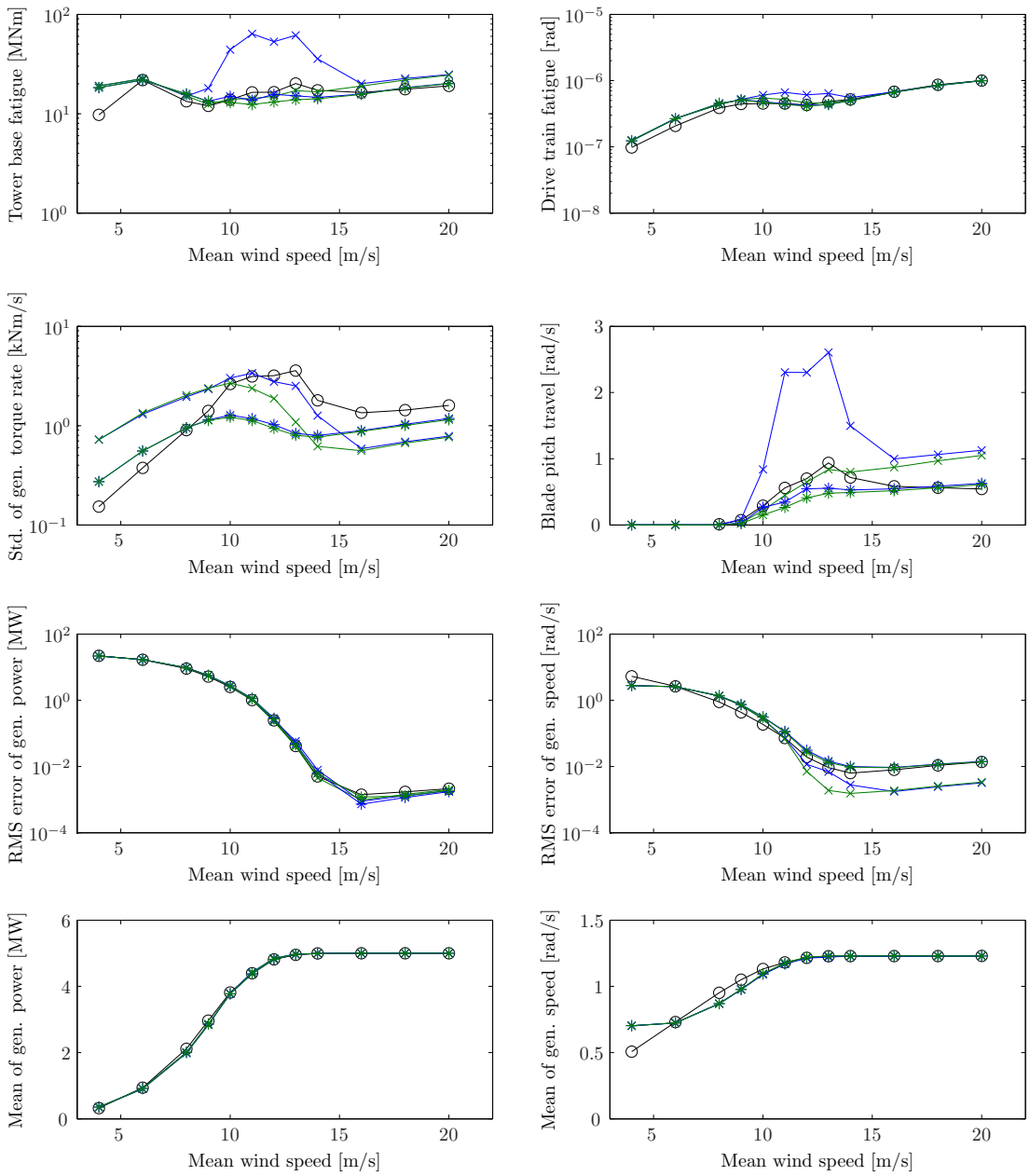

Figure 5: Performance metrics at a range of wind speeds. [○] PI controller. [×] MPC1 (baseline). [∗] MPC2 (reduced generator speed tracking weight). Results where the quasi-static aerodynamic model is used are shown in blue and results where the dynamic inflow model is used are shown in green.

tempting to mitigate loads via pitch actuation during partial load operation.

Acknowledgments

This work is supported by the CASED Project funded by grant DSF-09-063197 of the Danish Council for Strategic Research.

References

[1] S. Øye. Unsteady wake effects caused by pitch-angle changes. In *IEA R&D WECS Joint Action on Aerodynamics of Wind Turbines, 1st Symposium*, pages 58–79, London, United Kingdom, 1986.

[2] H. Snel and J. G. Schepers. Engineering models for dynamic inflow phenomena. *Journal of Wind Engineering and Industrial Aerodynamics*, 39(1-3):267–281, 1992.

[3] H. Snel and J. G. Schepers. Joint investigation

of dynamic inflow effects and implementation of an engineering method. Technical Report ECN-C–94-107, ECN Wind Energy, 1995.

[4] T. G. van Engelen and E. L. van der Hooft. Dynamic inflow compensation for pitch controlled wind turbines. In *European Wind Energy Conference*, London, United Kingdom, 2004.

[5] M. H. Hansen, A. H., T. J. Larsen, S. Øye, P. Sørensen, and P. Fuglsang. Control design for a pitch-regulated, variable speed wind turbine. Technical Report Risø-R-1500(EN), Risø National Laboratory, 2005.

[6] K. Z. Østergaard, J. Stoustrup, and P. Brath. Linear parameter varying control of wind turbines covering both partial load and full load conditions. *International Journal of Robust and Nonlinear Control*, 19(1):92–116, 2009.

[7] F. D. Bianchi, R. J. Mantz, and C. F. Christiansen. Gain scheduling control of variable-speed wind energy conversion systems using quasi-lpv models. *Control Engineering Practice*, 13(2):247 – 255, 2005.

[8] S. Bhowmik and R. Spee. Wind speed estimation based variable speed wind power generation. In *IECON '98. Proceedings of the 24th Annual Conference of the IEEE*, pages 596–601, Aachen, Germany, 1998. Industrial Electronics Society.

[9] E. L. van der Hooft and T. G. van Engelen. Estimated wind speed feed forward control for wind turbine operation optmisation. In *European Wind Energy Conference*, London, United Kingdom, 2004.

[10] K. Z. Østergaard, P. Brath, and J. Stoustrup. Estimation of effective wind speed. In *Journal of Physics: Conference Series*, volume 75, page 012082, Lyngby, Denmark, 2007. The Science of Making Torque from Wind.

[11] M. O. L. Hansen. *Aerodynamics of Wind Turbines*. Earthscan, second edition, 2008.

[12] N. N. Sørensen and H. A. Madsen. Modelling of transient wind turbine loads during pitch motion. In *European Wind Energy Conference*, Milan, Italy, 2007.

[13] T. J. Larsen and A. M. Hansen. How 2 HAWC2, the user's manual. Technical Report Risø-R-1597(ver. 3-1)(EN), Risø National Laboratory, 2007.

[14] R. P. Coleman and A. M. Feingold. Theory of self-excited mechanical oscillations of helicopter rotors with hinged blades. Technical Report 1351, National Advisory Committee for Aeronautics (NACA), 1958.

[15] G. Bir. Multi-blade coordinate transformation and its application to wind turbine analysis. In *46th AIAA aerospace sciences meeting and exhibit*, Reno, NV., 2008. [CD ROM].

[16] M. H. Hansen. Improved modal dynamics of wind turbines to avoid stall-induced vibrations. *Wind Energy*, 6(2):179–195, 2003.

[17] L. C. Henriksen, N. K. Poulsen, and H. H. Niemann. Constraint handling within a multi-blade coordinate framework of a wind turbine. In *Proceedings of the 50th IEEE Conference on Decision and Control and European Control Conference*, pages 5825–5830, Orlando, FL (US), 12-15 Dec 2011.

[18] L. Meirovitch. *Fundamentals of vibrations*. McGraw-Hill, 2001.

[19] J. Jonkman, S. Butterfield, W. Musial, and G. Scott. Definition of a 5-MW reference wind turbine for offshore system development. Technical Report NREL/TP-500-38060, National Renewable Energy Laboratory, 1617 Cole Boulevard, Golden, Colorado 80401-3393, February 2009.

[20] L. Kristensen and S. Frandsen. Model for power spectra of the blade of a wind turbine measured from the moving frame of reference. *Journal of Wind Engineering and Industrial Aerodynamics*, 10(2):249 – 262, 1982.

[21] H. Aa. Madsen, R. Mikkelsen, S. Øye, C. Bak, and J. Johansen. A detailed investigation of the blade element momentum (bem) model based on analytical and numerical results and proposal for modifications of the bem model. In *Journal of Physics: Conference Series 75: The Science of Making Torque from Wind*, Copenhagen, Denmark, 2007.

[22] L. C. Henriksen. *Model Predictive Control of Wind Turbines*. PhD thesis, Technical University of Denmark, Risø National Laboratory for Sustainable Energy, Wind Energy Division, 2010.

[23] J. Mann. Wind field simulation. *Probabilistic Engineering Mechanics*, 13(4):269–282, 1998.

[24] IEC/TC88. *IEC 61400-1 Ed.3: Wind turbines - Part 1: Design requirements*. International Electrotechnical Commission (IEC), 8 2005.

[25] *ASTM E1049 - 85(2005) Standard Practices for Cycle Counting in Fatigue Analysis*. ASTM International, 2005.